Editors' Suggestion | Featured in Physics

# Breaking the Intrinsic Absorption Limit for Arbitrarily Thin Conductive Films at Grazing Incidence

Yuxuan Liu,[1,*] Ren-Hao Fan,[2,3,*] Dong-Xiang Qi,[2] Ruwen Peng,[2,3,†] Yun Lai,[2,3,‡] Mu Wang,[2,3,§] and Jie Luo[1,3,‖]
[1]School of Physical Science and Technology, Jiangsu Key Laboratory of Frontier Material Physics and Devices, and Jiangsu Key Laboratory of Advanced Negative Carbon Technologies, Soochow University, Suzhou 215006, China
[2]National Laboratory of Solid State Microstructures, School of Physics, Collaborative Innovation Center of Advanced Microstructures, Nanjing University, Nanjing 210093, China
[3]Jiangsu Physical Science Research Center, Nanjing 210093, Nanjing, China

(Received 26 July 2025; revised 9 October 2025; accepted 3 December 2025; published 28 January 2026)

The absorption properties of ultrathin conductive films are of fundamental significance in electromagnetics and photonics, impacting applications from radar stealth to two-dimensional material optoelectronics. For decades, a 50% absorption limit has been considered intrinsic to such films in symmetric environments, regardless of frequency or incident angle. Here, we demonstrate the breaking of this long-standing limit under grazing incidence, where the absorption was regarded as negligible due to extreme impedance mismatch. We reveal a previously unknown absorption limit of $2\sqrt{2}-2\approx 82.8\%$ for grazing transverse-magnetic waves on arbitrarily thin, highly conductive films. This exceptional absorption arises from a pseudo-Brewster effect with minimal reflection $3-2\sqrt{2}\approx 17.2\%$ and vanishing skin depth of grazing waves. Remarkably, the enhanced absorption is sustained across an ultrabroad frequency range. Terahertz experiments using deep-subwavelength doped silicon wafers validate our theoretical predictions. These findings fundamentally advance our understanding of wave-matter interactions at deep-subwavelength scales and pave the way for extreme-angle photonic and electromagnetic devices.

DOI: 10.1103/71vr-lb26

Efficient electromagnetic wave-absorbing films are crucial for a wide range of applications, from multispectral electromagnetic shielding and radar stealth [1–5] to terahertz detection and imaging [6], as well as optoelectronic modulation and detection in the infrared and visible regimes [7–9]. The emergence of two-dimensional (2D) materials such as graphene and transition metal dichalcogenides, characterized by nearly free electrons, has enabled strong light–matter interactions at deep-subwavelength scales [10,11]. Their ultrathin profiles and exceptional optoelectronic properties are increasingly important for device miniaturization, weight reduction, and system integration in applications including microwave absorbers [3,4] and next-generation optoelectronics [8,9]. Yet, their extreme thinness fundamentally constrains absorption efficiency, raising a central question: *What is the ultimate absorption limit of an arbitrarily thin, homogeneous, nonmagnetic conductive film, such as a 2D material sheet?*

This fundamental question has been extensively studied, with textbooks and literatures establishing a 50% absorption limit for ultrathin films in symmetric environments, which is also known as the intrinsic thin-film absorption limit [5,12–25]. Recent advances in 2D materials have focused on approaching this theoretical maximum across broad bandwidths [5,18–25]. Notably, this 50% absorption limit originates from a fundamental physical constraint: the continuity of tangential electric fields across infinitesimally thin films [17]. For symmetric configurations, the relation between reflection coefficient $r$ and transmission coefficient $t$ is $1+r=t$, which imposes an upper bound of 50% on absorption ($A=1-|r|^2-|t|^2$), with the maximum achieved under the condition $t=-r=0.5$ [17]. In this well-established framework, the 50% absorption limit is generally regarded as independent of frequency, polarization, and angle of incidence [25].

Here, we challenge this 50% absorption limit for arbitrarily thin conductive films in symmetric environments, and report a maximum absorption of $2\sqrt{2}-2\approx 82.8\%$ for transverse-magnetic (TM) polarization under grazing incidence (i.e., incident angle approaches 90°), for the first time to the best of our knowledge. The absorption in this scenario was thought negligible due to near-unity Fresnel reflection coefficients [26]. This breakthrough occurs because the requirement of $1+r=t$ no longer holds at grazing incidence, despite the tangential electric fields remain near-uniform across the film. Remarkably, the absorption maintains above the conventional 50% limit

*These authors contributed equally to this work.
†Contact author: rwpeng@nju.edu.cn
‡Contact author: laiyun@nju.edu.cn
§Contact author: muwang@nju.edu.cn
‖Contact author: luojie@suda.edu.cn

 

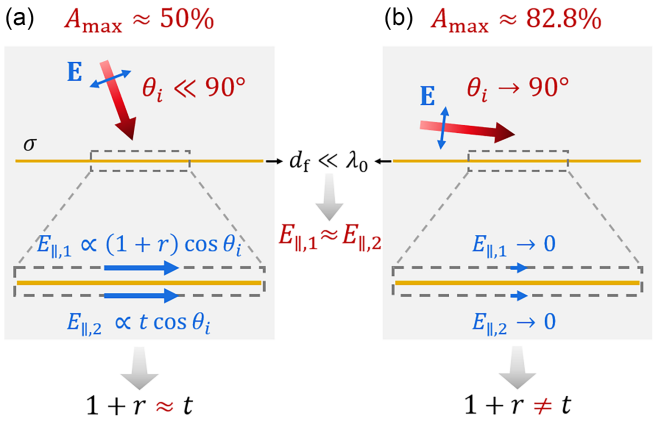


FIG. 1. Schematic of TM wave absorption by an ultrathin conductive film (e.g., 2D material) in a symmetric environment. (a) At small-angle incidence ($\theta_i \ll 90°$), nearly uniform tangential electric fields ($E_{\parallel,1} \approx E_{\parallel,2}$) enforce $1 + r \approx t$, limiting maximum absorption to 50%. (b) At grazing incidence ($\theta_i \to 90°$), while $E_{\parallel,1} \approx E_{\parallel,2}$ persists, field magnitudes vanish ($E_{\parallel,1}, E_{\parallel,2} \propto \cos\theta_i \to 0$), relaxing the constraint $1 + r \approx t$ and enabling 82.8% maximum absorption.

over an ultrabroad frequency range. Terahertz experiments using deep-subwavelength doped silicon wafers validate the theoretical predictions. By rewriting the conventional absorption limit, our findings hold far-reaching implications for radar stealth and optoelectronic modulation and detection technologies.

Let us start from an ultrathin nonmagnetic conductive film (conductivity $\sigma$, relative permeability $\mu_f = 1$) placed in a symmetric environment, as illustrated in Fig. 1. Its relative permittivity $\varepsilon_f$ is given by $\varepsilon_f = 1 + i(\sigma/\omega\varepsilon_0)$, where $\omega$ is the angular frequency and $\varepsilon_0$ is the permittivity of vacuum. The film thickness $d_f$ is much smaller than free-space wavelength $\lambda_0$, i.e., $d_f \ll \lambda_0$. We consider the incidence of a TM plane wave, characterized by in-plane electric fields under an incident angle of $\theta_i$. A time variation term of $e^{-i\omega t}$ is assumed throughout this Letter.

To explore the relationship between electric fields on the upper and lower surfaces of the film, we apply the Maxwell-Faraday equation $\oint \mathbf{E} \cdot d\mathbf{l} = i\omega \iint \mathbf{B} \cdot d\mathbf{S}$ to a very thin Amperian loop that straddles the film, as depicted by the gray dashed lines in Fig. 1. In the limit where the loop's height goes to the deep-subwavelength scale (i.e., $d_f \ll \lambda_0$), the term $i\omega \iint \mathbf{B} \cdot d\mathbf{S}$ becomes negligible, leading to $\oint \mathbf{E} \cdot d\mathbf{l} \approx 0$. At the same time, the contribution of the normal electric field to $\oint \mathbf{E} \cdot d\mathbf{l}$ can be ignored. Consequently, we obtain

$$E_{\parallel,1} \approx E_{\parallel,2}, \tag{1}$$

where $E_{\parallel,1}$ and $E_{\parallel,2}$ are the tangential electric fields on the upper and lower boundaries of the loop, respectively. Equation (1) indicates that the tangential electric fields are near-uniform across the film.

Assuming the incident electric-field amplitude as $E_0$, the tangential electric fields can be expressed as $E_{\parallel,1} = E_0(1 + r)\cos\theta_i$ and $E_{\parallel,2} = E_0 t\cos\theta_i$, where $r$ and $t$ are the reflection and transmission coefficients, respectively. Substituting these into Eq. (1) yields

$$(1 + r)\cos\theta_i \approx t\cos\theta_i. \tag{2}$$

For small-angle incidence ($\theta_i \ll 90°$), Eq. (2) simplifies to

$$1 + r \approx t. \tag{3}$$

For a film in a symmetric environment, the absorption is given as $A = 1 - |r|^2 - |t|^2$. An important consequence of Eq. (3) is that the maximum absorption is 50%, that is, $A_{\max} = 50\%$, occurring under the condition $t = -r = 0.5$, which is referred as the intrinsic thin-film absorption limit [5,12–25].

Conventionally, this 50% absorption limit holds in two conditions: (i) a symmetric environment and (ii) near-uniform tangential electric fields across the film. Breaking this limit requires either symmetry breaking (e.g., through asymmetric substrates or reflectors [16,17,27–32]) or strong magnetic responses, such as those arising from magnetic materials (e.g., cobalt, iron, and nickel compounds [3,4]) or effective magnetic resonances (e.g., those mediated by electric displacement currents in high-index meta-atoms [33–38]). For reflector configurations, 100% absorption can occur under critical coupling or resonant conditions [16,17,28–32], as in the Salisbury screen [27]. Magnetic mechanisms, on the other hand, can enable 100% absorption by disrupting tangential field uniformity and ensuring impedance matching with free space [3,4,33–38]. Additionally, coherent illumination (e.g., using two coherent counterpropagating beams) offers a third pathway, functionally analogous to employing perfect electric or magnetic reflectors [17,39,40]. A comparative summary of these strategies is provided in Supplemental Material [41].

Remarkably, we discover that the 50% absorption limit can be surpassed at grazing incidence ($\theta_i \to 90°$), while preserving both symmetry and field uniformity [Fig. 1(b)]. This breakthrough occurs because $\cos\theta_i \to 0$ as $\theta_i \to 90°$, naturally fulfilling $E_{\parallel,1} \approx E_{\parallel,2} \approx 0$ [Eq. (1)] without requiring $1 + r \approx t$ [Eq. (3)]. In this scenario, we have

$$1 + r \neq t. \tag{4}$$

Equation (4) unlocks the potential for surpassing the 50% absorption limit. As shown below, a maximum absorption of 82.8% can be attained at grazing incidence.

For demonstration, we consider a 10 μm-thick conductive film (conductivity $\sigma$) suspended in free space and illuminated by a TM wave under an incident angle of $\theta_i$

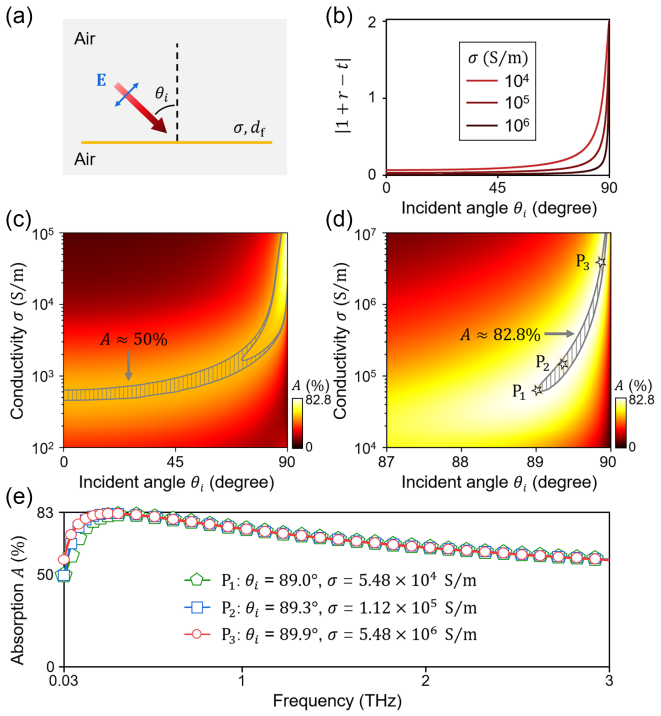


FIG. 2. (a) Schematic of TM wave absorption by an ultrathin conductive film (conductivity $\sigma$, thickness $d_f$) suspended in free space. (b) Computed $|1+r-t|$ for a 10 μm-thick film as a function of $\theta_i$ at 0.3 THz for varying $\sigma$. (c) Absorption $A$ of the 10 μm-thick film with respect to $\theta_i$ and $\sigma$ at 0.3 THz, with the gray region marking $A \approx 50\%$. (d) Absorption $A$ for large values of $\theta_i$ and $\sigma$, where the gray region indicates $A \approx 82.8\%$. (e) Absorption spectra for points $P_1$ ($\theta_i = 89.0°$, $\sigma = 5.48 \times 10^4$ S/m), $P_2$ ($\theta_i = 89.3°$, $\sigma = 1.12 \times 10^5$ S/m), and $P_3$ ($\theta_i = 89.9°$, $\sigma = 5.48 \times 10^6$ S/m), as marked in (d).

[Fig. 2(a)]. The film is ultrathin compared to the operating wavelength of 1 mm corresponding to a frequency of 0.3 THz. Figure 2(b) presents the values of $|1+r-t|$ for this film as a function of $\theta_i$ at 0.3 THz for $\sigma = 10^4$–$10^6$ S/m, calculated using the transfer matrix method [42]. Evidently, at small angle of incidence, the condition $1+r \approx t$ is valid. However, as $\theta_i$ approaches 90°, this relation breaks down severely, irrespective of $\sigma$. This breakdown, consistent with our theoretical prediction, allows for absorption to exceed the 50% limit. The absorption map as a function of $\theta_i$ and $\sigma$ at 0.3 THz [Fig. 2(c)] confirms this phenomenon. While small angles exhibit the expected 50% absorption limit (gray-shaded area), larger $\theta_i$ combined with higher $\sigma$ yields unprecedented absorption (> 50%). Strikingly, the absorption peaks at ~82.8% [gray-shaded area in Fig. 2(d)] under near-grazing incidence. Three representative cases, marked in Fig. 2(d) as points $P_1$ ($\theta_i = 89.0°$, $\sigma = 5.48 \times 10^4$ S/m), $P_2$ ($\theta_i = 89.3°$, $\sigma = 1.12 \times 10^5$ S/m), and $P_3$ ($\theta_i = 89.9°$, $\sigma = 5.48 \times 10^6$ S/m, further demonstrate this enhanced absorption. Their absorption spectra [Fig. 2(e)] maintain above 50% across an exceptionally broad frequency range (e.g., 0.03 ~ 3 THz for $P_3$). It is important to note that the bandwidth broadens as $\theta_i$ gets closer to 90°. These results clearly show the breakdown of the conventional 50% absorption limit for ultrathin conductive films under grazing incidence, achieving a maximum absorption of 82.8%.

The 82.8% absorption limit at grazing incidence can be rigorously derived using the transfer matrix method [42]. For ultrathin films satisfying $d_f \ll \lambda_0$, the reflection and transmission coefficients can be expressed as follows:

$$r = -\frac{(i+\gamma^2)\sin\sqrt{i\beta}}{2\sqrt{i}\gamma\cos\sqrt{i\beta} + (-i+\gamma^2)\sin\sqrt{i\beta}}, \tag{5}$$

$$t = \frac{2\sqrt{i}\gamma}{2\sqrt{i}\gamma\cos\sqrt{i\beta} + (-i+\gamma^2)\sin\sqrt{i\beta}}, \tag{6}$$

where $\beta = \sigma\omega\mu_0 d_f^2$ and $\gamma = \sqrt{(\sigma/\omega\varepsilon_0)}\cos\theta_i$; $\mu_0$ is the permeability of vacuum.

The absorption $A$, calculated as $1 - |r|^2 - |t|^2$, can then be derived as

$$A = 1 - \frac{-8\gamma^2 + (1+\gamma^4)(\cos\sqrt{2\beta} - \cosh\sqrt{2\beta})}{(1-4\gamma^2+\gamma^4)\cos\sqrt{2\beta} - (1+4\gamma^2+\gamma^4)\cosh\sqrt{2\beta} + 2\sqrt{2}(\gamma-\gamma^3)\sin\sqrt{2\beta} - 2\sqrt{2}(\gamma+\gamma^3)\sinh\sqrt{2\beta}}. \tag{7}$$

The absorption $A$ is maximized when

$$\omega\varepsilon_0 = \sigma\cos^2\theta_i \quad \text{and} \quad \cos\theta_i \ll k_0 d_f \ll 1. \tag{8}$$

Substituting into Eq. (7) reveals the absorption limit,

$$A_{\max} = 2\sqrt{2} - 2 \approx 82.8\%. \tag{9}$$

This solution yields $r = i(1-\sqrt{2})$ and $t = 0$, which significantly differ from the condition $1 + r \approx t$ [Eq. (3)] for traditional small-angle scenarios. The detailed derivation is summarized in Supplemental Material [41]. Our analysis establishes that ultrathin conductive films satisfying Eq. (8) can reach the theoretical absorption limit of 82.8%, with the film thickness $d_f$ becoming arbitrarily small compared to operating wavelength as $\theta_i \to 90°$.

The enhanced absorption of grazing TM waves presents a seeming contradiction. Traditional theory predicts near-total reflection and negligible absorption at grazing incidence due to both extreme impedance mismatch (driving

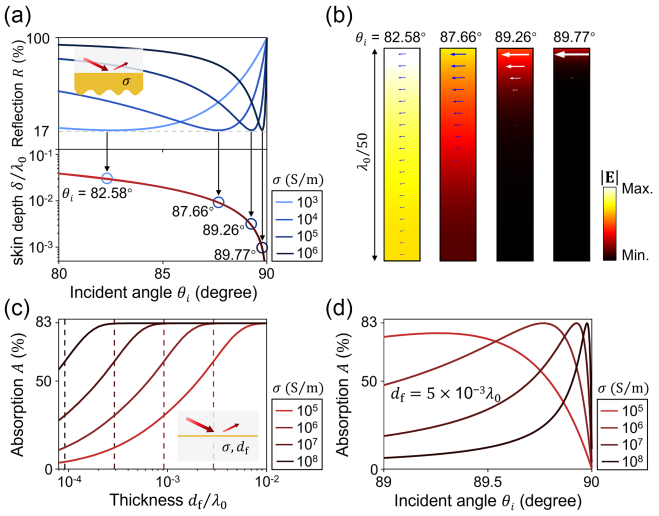


FIG. 3. (a) Reflection $R$ (upper) and normalized skin depth $\delta/\lambda_0$ (lower) for a semi-infinite conductor in free space (inset) as a function of $\theta_i$ for TM waves at 0.3 THz for varying $\sigma$. Reflection minima occur at $\theta_i = 82.58°$, 87.66°, 89.26°, and 89.77° for different $\sigma$. (b) Simulated electric-field amplitude $|\mathbf{E}|$ (color map) and current density $\mathbf{J}$ (blue and white arrows) within the semi-infinite conductor for the four reflection-minimum cases marked in (a). The current density arrows are scaled down by factors of $3^0$, $3^1$, $3^2$, and $3^3$ from left to right. The incident power along the vertical direction for the four cases is identical. (c) Absorption $A$ of a conductive film suspended in free space (inset) versus normalized thickness $d_f/\lambda_0$ at 0.3 THz for varying $\sigma$, with $\theta_i = \arccos\sqrt{\omega\varepsilon_0/\sigma}$ to minimize reflection. Dashed lines indicate skin depths for each $\sigma$ case. (d) Absorption $A$ for the conductive film of fixed thickness $5 \times 10^{-3}\lambda_0$ as a function of $\theta_i$ at 0.3 THz for varying $\sigma$.

Fresnel coefficients to unity) [26] and vanishing tangential electric field $E_\parallel \propto \cos\theta_i \to 0$, which governs thin-film absorption [43–45]. Surprisingly, in our Letter, we unexpectedly report strong broadband absorption enhancement. This contradiction is resolved when considering the extremely high conductivity $\sigma \propto \cos^{-2}\theta_i$ [Eq. (8)], which compensates for the diminished $E_\parallel$ to maintain a substantial tangential current $J_\parallel = \sigma E_\parallel \propto \cos^{-1}\theta_i$, thereby enabling efficient energy dissipation.

Notably, the extremely high conductivity $\sigma$ renders the film a near-perfect conductor—a condition typically associated with unity Fresnel reflection coefficients [26]. While transverse-electric waves indeed undergo near-total reflection under these conditions [36], we observe a striking contrast for TM waves at grazing incidence: rather than total reflection, the high conductivity enables low reflection with strong absorption. This counterintuitive response reveals the fundamental mechanism behind the 82.8% absorption limit. To clarify this mechanism, we analyze a semi-infinite conductor (conductivity $\sigma$) in free space, as illustrated by the inset in Fig. 3(a). According to Fresnel's equations for TM waves under good-conductor condition ($\sigma \gg \omega\varepsilon_0$) [26], we derive the reflection $R$ on the conductor's surface:

$$R = \frac{\omega^2\varepsilon_0^2 + \sigma^2\cos^4\theta_i}{(\omega\varepsilon_0 + \sqrt{2\sigma\omega\varepsilon_0}\cos\theta_i + \sigma\cos^2\theta_i)^2}. \tag{10}$$

The reflection $R$ attains its minimal value of

$$R_{\min} = 3 - 2\sqrt{2} \approx 17.2\%, \tag{11}$$

when

$$\omega\varepsilon_0 = \sigma\cos^2\theta_i \quad \text{and} \quad \cos\theta_i \ll 1. \tag{12}$$

Under these conditions, the skin depth within the conductor is expressed as

$$\delta = \sqrt{\frac{2}{\omega\sigma\mu_0}} = \sqrt{2}\frac{\cos\theta_i}{k_0}. \tag{13}$$

The detailed derivation is summarized in Supplemental Material [41]. Equations (11)–(13) reveal a minimal reflection of 17.2% for grazing TM waves on a near-perfect conductor with extremely high $\sigma$, accomplished by a vanishing skin depth (i.e., $\delta \to 0$) when $\theta_i \to 90°$. We note that this minimal reflection can be alternatively understood as a manifestation of the pseudo-Brewster effect [46,47], corresponding to minimal reflection on lossy materials. In contrast to previous studies, which predominantly focused on low-conductivity materials at moderate incident angles [46,47], our Letter represents the first demonstration of a 17.2% minimal reflection for good conductors under grazing incidence. This finding challenges the conventional expectation of near-perfect reflection for good conductors [26], offering new insights into wave-matter interactions at extreme configurations.

The numerical verification is presented in Fig. 3(a), where the reflection $R$ (upper panel) and normalized skin depth $\delta/\lambda_0$ (lower panel) on the semi-infinite conductor for different values of $\sigma$ and $\theta_i$ at 0.3 THz are calculated. Evidently, the reflection minima of 17.2% occur at specific $(\sigma, \theta_i)$ pairs ($10^3$ S/m at 82.58°, $10^4$ S/m at 87.66°, $10^5$ S/m at 89.26°, and $10^6$ S/m at 89.77°), each satisfying $\omega\varepsilon_0 = \sigma\cos^2\theta_i$. Simultaneously, the skin depth is observed to significantly decrease as $\theta_i$ approaches 90°. These unusual wave behaviors are further visualized in numerical simulations shown in Fig. 3(b), obtained using software COMSOL Multiphysics. The distributions of electric-field amplitude $|\mathbf{E}|$ (color map) and current density $\mathbf{J}$ (arrows) within the semi-infinite conductor corresponding to the four reflection minimum cases reveal two critical features: first, the fields decay more rapidly as $\theta_i \to 90°$, consistent with the vanishing skin depth; second, the initial current becomes proportionally larger, maintaining constant

absorption despite reduced field penetration. As demonstrated in Supplemental Material [41], besides 17.2% of incident energy being reflected, the remaining 82.8% is absorbed via Ohmic dissipation in the conductor (arising from the tangential electric fields and the associated currents), consistent with energy conservation. These observations demonstrate how the conductor's extreme $\sigma$ compensates for diminished field penetration by enhancing the current density, explaining the persistence of low reflection at grazing angles.

The transition from bulk to thin-film behavior occurs upon truncating the semi-infinite conductor at a depth $d_\mathbf{f} \gg \delta$. This creates a conductive film where the thickness condition $d_\mathbf{f} \gg \delta$ ensures complete suppression of transmission, reducing the absorption to $A = 1 - R$. Consequently, the maximal absorption $A_{\max} = 1\text{–}17.2\% = 82.8\%$ emerges directly from the minimal reflection $R_{\min} = 17.2\%$, perfectly matching our observations for ultrathin conductive films at grazing incidence. As previously shown, at the 82.8% absorption limit, the reflection and transmission coefficients are $r = i(1 - \sqrt{2})$ and $t = 0$ [Eqs. (5) and (6)], yielding a reflection of $R = |r|^2 \approx 17.2\%$ and zero transmission. The physical picture becomes complete when considering the thickness requirement $d_\mathbf{f} \gg \delta$ that imposes $k_0 d_\mathbf{f} \gg \cos\theta_i$ according to Eq. (13). When combined with the constraints in Eq. (12), this precisely yields the conditions for the 82.8% absorption limit in Eq. (8). This mathematical consistency confirms that the 82.8% absorption limit in ultrathin conductive films fundamentally originates from two synergistic mechanisms: (i) the occurrence of pseudo-Brewster effect with minimal reflection (17.2%), and (ii) the vanishing skin depth. Crucially, as $\theta_i \to 90°$, we have $\delta \to 0$ [Eq. (13)], making the 82.8% absorption limit achievable in films of arbitrarily small thickness relative to operating wavelength.

To further validate these findings, we explore the absorption properties of a conductive film (thickness $d_\mathrm{f}$, conductivity $\sigma$) suspended in free space for TM waves at 0.3 THz [Fig. 3(c), inset]. Figure 3(c) shows the absorption as a function of the normalized thickness $d_\mathbf{f}/\lambda_0$ for various $\sigma$ values, with $\theta_i = \arccos\sqrt{\omega\varepsilon_0/\sigma}$ [Eq. (12)] for each $\sigma$ case to ensure the occurrence of pseudo-Brewster effect. It is evident that the 82.8% absorption limit is reached when $d_\mathrm{f}$ exceeds several skin depths (dashed lines)—a threshold thickness that decreases sharply with increasing $\sigma$. Then, we fix $d_\mathrm{f}$ at $5 \times 10^{-3}\lambda_0$ and calculate the absorption as a function of $\theta_i$ with varying $\sigma$, as shown in Fig. 3(d). We see that as $\sigma$ increases, the absorption maxima increase and shift toward larger $\theta_i$, ultimately reaching the 82.8% absorption limit when the skin depth is much smaller than the film thickness. These numerical results verify that the 82.8% absorption limit occurs when the pseudo-Brewster effect appears with a minimal reflection 17.2% and the thickness condition $d_\mathbf{f} \gg \delta$ is satisfied, which is in excellent agreement with the above theoretical predictions.

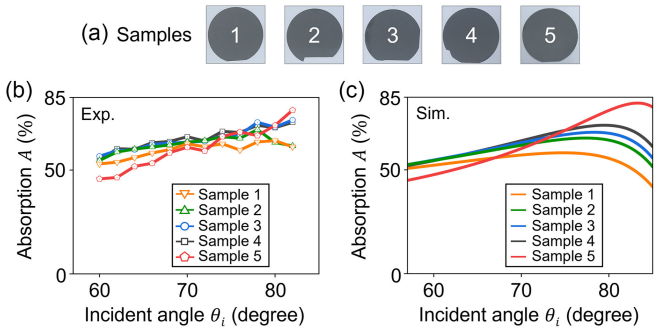


FIG. 4. (a) Photographs of five doped silicon wafers (thickness ~75 μm) with different conductivities: 153 S/m (sample 1), 220 S/m (sample 2), 257 S/m (sample 3), 315 S/m (sample 4), and 790 S/m (sample 5). (b) Measured and (c) simulated absorption $A$ as the function of $\theta_i$ for TM waves at 0.2 THz for each sample.

Subsequently, we conduct terahertz experiments to validate our thin-film absorption theory. While direct observation of the 82.8% absorption limit at extreme angles ($> 80°$) presents significant challenges [48,49], Fig. 3(d) reveals a crucial trend: for films of a fixed thickness, absorption maxima increase and shift toward larger incident angles as the conductivity increases. This behavior provides an experimentally accessible pathway to verify our theory. To capture this trend, we fabricated five deep-subwavelength doped silicon wafers (thickness ~75 μm) with different conductivity $\sigma$ [Fig 4(a)]. Figure 4(b) presents the measured absorption within the incident angle range of $60° \sim 82°$ at 0.2 THz, showing excellent agreement with simulations [Fig 4(c)]. The minor observed discrepancies likely originate from sample-related uncertainties (thickness and conductivity variations), as well as measurement errors (residual wave leakage, incident angle alignment, and random errors), with detailed methodologies and error analysis provided in Supplemental Material [41]. Experimental and simulation results confirm both the violation of the 50% absorption limit and the predicted trend of increasing and angle-shifting absorption maxima with rising $\sigma$. Notably, sample 5 with the highest conductivity exhibits an absorption closer to the theoretical limit. We further note that the finite thickness of real silicon wafers shifts the critical angle for exceeding 50% absorption toward smaller incident angles and slightly elevates the absorption. These experimental results provide strong support for our thin-film absorption theory.

It is noteworthy that the observed absorption enhancement in deep-subwavelength films operates universally across spectral regimes. At microwave frequencies, a conductive film ($d_\mathbf{f} \approx 0.38$ mm, $\sigma \approx 1.8 \times 10^3$ S/m) reaches 82.8% absorption at 10 GHz under $\theta_i = 89°$, sustaining $> 50\%$ absorption across an exceptional bandwidth ($1 \sim 100$ GHz). Such films can be readily implemented using conductive composites like indium tin oxide

and metallic filaments [44,45,50], with significant applications in stealth technologies and electromagnetic shielding [1–5]. Strikingly, this phenomenon scales to terahertz and infrared regimes, where a ∼126 nm-thick film with $\sigma \approx 5.5 \times 10^6$ S/m achieves identical peak absorption (82.8%) at 10 μm wavelength under $\theta_i = 89°$, with broadband high absorption (> 50%) spanning $1 \sim 100$ μm [41]. Noble metals (e.g., silver and gold [51]) and emerging 2D materials (e.g., Mxenes [5,20,24]) meet these requirements, enabling applications in terahertz modulators [52] and wide-angle photodetectors [9]. A comprehensive material selection guideline spanning spectral regimes is provided in Supplemental Material [41], highlighting the universality of our thin-film absorption theory.

In conclusion, we have demonstrated both theoretically and experimentally that ultrathin conductive films can surpass the intrinsic 50% absorption limit. Our Letter reveals a previously unknown absorption limit of 82.8% for grazing TM waves on arbitrarily thin, high-conductivity films, originating from the pseudo-Brewster effect with minimal reflection 17.2% and vanishing skin depth on such films. This discovery provides crucial insights into wave-matter interactions at deep-subwavelength scales and hold significant potential for high-performance devices at extreme angles.

*Acknowledgments*—This work was supported by the National Key R&D Program of China (Grant No. 2022YFA1404303), the National Natural Science Foundation of China (Grant Nos. 12234010, 12374293, 12474293, 12174188), and the Natural Science Foundation of Jiangsu Province (Grants No. BK20233001, No. BK20221438, and No. BK20221354).

*Data availability*—The data are not publicly available. The data are available from the authors upon reasonable request.

[1] Y. Ra'di, C. R. Simovski, and S. A. Tretyakov, Thin perfect absorbers for electromagnetic waves: Theory, design, and realizations, Phys. Rev. Appl. **3**, 037001 (2015).
[2] S. Qu and P. Sheng, Microwave and acoustic absorption metamaterials, Phys. Rev. Appl. **17**, 047001 (2022).
[3] J. Li, D. Zhou, P. Wang, C. Du, W. Liu, J. Su, L. Pang, M. Cao, and L. Kong, Recent progress in two-dimensional materials for microwave absorption applications, Chem. Eng. J. (Lausanne) **425**, 131558 (2021).
[4] Y. Wang, L. Zhu, L. Han, X. Zhou, Y. Gao, and L. Lv, Recent progress of one-dimensional nanomaterials for microwave absorption: A review, ACS Appl. Nano Mater. **6**, 7107 (2023).
[5] A. Iqbal, T. Hassan, S. M. Naqvi, Y. Gogotsi, and C. M. Koo, MXenes for multispectral electromagnetic shielding, Nat. Rev. Electr. Eng. **1**, 180 (2024).
[6] H. T. Chen, J. F. O'Hara, A. K. Azad, and A. J. Taylor, Manipulation of terahertz radiation using metamaterials, Laser Photonics Rev. **5**, 513 (2011).
[7] L. Feng, P. Huo, Y. Liang, and T. Xu, Photonic metamaterial absorbers: Morphology engineering and interdisciplinary applications, Adv. Mater. **2019**, 1903787 (2019).
[8] C. Liu, J. Guo, L. Yu, J. Li, M. Zhang, H. Li, Y. Shi, and D. Dai, Silicon /2D-material photodetectors: From near-infrared to mid-infrared, Light-Sci. Appl. **10**, 123 (2021).
[9] Z. Li, T. Yan, and X. Fang, Low-dimensional wide-bandgap semiconductors for UV photodetectors, Nat. Rev. Mater. **8**, 587 (2023).
[10] M. Xu, T. Liang, M. Shi, and H. Chen, Graphene-like two-dimensional materials, Chem. Rev. **113**, 3766 (2013).
[11] F. Xia, H. Wang, D. Xiao, M. Dubey, and A. Ramasubramaniam, Two-dimensional material nanophotonics, Nat. Photonics **8**, 899 (2014).
[12] W. Woltersdorff, Uber die optischen Konstanten diinner MetaUschichten im langwelligen Ultrarot, Z. Phys. **91**, 230 (1934).
[13] L. N. Hadley and D. M. Dennison, Reflection and transmission interference filters, J. Opt. Soc. Am. **37**, 451 (1947).
[14] C. Hilsum, Infrared absorption of thin metal films, J. Opt. Soc. Am. **44**, 188 (1954).
[15] B. A. Munk, *Frequency Selective Surfaces* (Wiley, New York, 2000).
[16] S. Thongrattanasiri, F. H. L. Koppens, and F. J. García De Abajo, Complete optical absorption in periodically patterned graphene, Phys. Rev. Lett. **108**, 047401 (2012).
[17] J. Luo, S. Li, B. Hou, and Y. Lai, Unified theory for perfect absorption in ultrathin absorptive films with constant tangential electric or magnetic fields, Phys. Rev. B **90**, 165128 (2014).
[18] P. H. Q. Pham, W. Zhang, N. V. Quach, J. Li, W. Zhou, D. Scarmardo, E. R. Brown, and P. J. Burke, Broadband impedance match to two-dimensional materials in the terahertz domain, Nat. Commun. **8**, 2233 (2017).
[19] N. Luhmann, D. Høj, M. Piller, H. Kähler, M. Chien, R. G. West, U. L. Andersen, and S. Schmid, Ultrathin 2 nm gold as impedance-matched absorber for infrared light, Nat. Commun. **11**, 2161 (2020).
[20] T. Zhao, P. Xie, H. Wan, T. Ding, M. Liu, J. Xie, E. Li, X. Chen, T. Wang, Q. Zhang, Y. Wei, Y. Gong, Q. Wen, M. Hu, C. Qiu, and X. Xiao, Ultrathin MXene assemblies approach the intrinsic absorption limit in the 0.5–10 THz band, Nat. Photonics **17**, 622 (2023).
[21] W. Fei, J. Li, L. Ma, T. Zhou, X. Zhu, X. He, S. Liu, J. Bian, and Q. Zhao, Electrochemically-switched microwave response of MXene in organic electrolyte, Adv. Mater. **36**, 2413311 (2024).
[22] Y. Guo, Z. Chen, Z. Jin, X. Wang, C. Zhang, A. V. Balakin, A. P. Shkurinov, Y. Peng, Y. Zhu, and S. Zhuang, Dynamically controllable terahertz electromagnetic interference shielding by small polaron responses in Dirac semimetal $PdTe_2$ thin films, Adv. Funct. Mater. **34**, 2407749 (2024).
[23] N. Qiu, X. Zhou, Q. Huang, J. Ye, and S. Du, Multifunctional $Yb_3Si_2C_2$ with high-performance terahertz shielding for future 6G communications, Adv. Funct. Mater. **34**, 2405747 (2024).

[24] T. Zhao, H. Wan, T. Zhang, and X. Xiao, Mechanism of the terahertz wave-MXene interaction and surface/interface chemistry of MXene for terahertz absorption and shielding, Acc. Chem. Res. **57**, 2184 (2024).
[25] R. Rakhmanov, S. Ippolito, M. Downes, A. Inman, J. AlHourani, J. Fitzpatrick, Y. Gogotsi, and G. Friedman, Influence of MXene interlayer spacing on the interaction with microwave radiation, Adv. Funct. Mater. **35**, 2410591 (2025).
[26] J. D. Jackson, *Classical Electrodynamics* (Wiley, New York, 1975), 3 ed.
[27] W. W. Salisbury, Absorbent body of electromagnetic waves, U.S. Patent No. 2,599,944, 1952.
[28] M. A. Kats, R. Blanchard, P. Genevet, and F. Capasso, Nanometre optical coatings based on strong interference effects in highly absorbing media, Nat. Mater. **12**, 20 (2013).
[29] J. R. Piper and S. Fan, Total absorption in a graphene monolayer in the optical regime by critical coupling with a photonic crystal guided resonance, ACS Photonics **1**, 347 (2014).
[30] C. A. Valagiannopoulos, A. Tukiainen, T. Aho, T. Niemi, M. Guina, and S. A. ô. S. Tretyakov, Perfect magnetic mirror and simple perfect absorber in the visible spectrum, Phys. Rev. B **91**, 115305 (2015).
[31] Z. Sakotic, A. Ware, M. Povinelli, and D. Wasserman, Perfect absorption at the ultimate thickness limit in planar films, ACS Photonics **10**, 4244 (2023).
[32] N. Kakenov, O. Balci, T. Takan, V. A. Ozkan, H. Altan, and C. Kocabas, Observation of gate-tunable coherent perfect absorption of terahertz radiation in graphene, ACS Photonics **9**, 1531 (2016).
[33] Y. Ra Di, V. S. Asadchy, S. U. Kosulnikov, M. M. Omelyanovich, D. Morits, A. V. Osipov, C. R. Simovski, and S. A. Tretyakov, Full light absorption in single arrays of spherical nanoparticles, ACS Photonics **2**, 653 (2015).
[34] N. Odebo Länk, R. Verre, P. Johansson, and M. Käll, Large-scale silicon nanophotonic metasurfaces with polarization independent near-perfect absorption, Nano Lett. **17**, 3054 (2017).
[35] H. K. Shamkhi, A. Sayanskiy, A. C. Valero, A. S. Kupriianov, P. Kapitanova, Y. S. Kivshar, A. S. Shalin, and V. R. Tuz, Transparency and perfect absorption of all-dielectric resonant metasurfaces governed by the transverse Kerker effect, Phys. Rev. Mater. **3**, 085201 (2019).
[36] W. Liu and Y. S. Kivshar, Generalized Kerker effects in nanophotonics and meta-optics, Opt. Express **26**, 13085 (2018).
[37] M. Chen, M. Kim, A. M. H. Wong, and G. V. Eleftheriades, Huygens' metasurfaces from microwaves to optics: A review, Nanophotonics **7**, 1207 (2018).
[38] R. Masoudian Saadabad, L. Huang, and A. E. Miroshnichenko, Polarization-independent perfect absorber enabled by quasibound states in the continuum, Phys. Rev. B **104**, 235405 (2021).
[39] S. Li, J. Luo, S. Anwar, S. Li, W. Lu, Z. H. Hang, Y. Lai, B. Hou, M. Shen, and C. Wang, Broadband perfect absorption of ultrathin conductive films with coherent illumination: Superabsorption of microwave radiation, Phys. Rev. B **91**, 220301(R) (2015).
[40] D. Yan, A. S. Shalin, Y. Wang, Y. Lai, Y. Xu, Z. H. Hang, F. Cao, L. Gao, and J. Luo, Ultrasensitive higher-order exceptional points via non-Hermitian zero-index materials, Phys. Rev. Lett. **134**, 243802 (2025).
[41] See Supplemental Material at http://link.aps.org/supplemental/10.1103/71vr-lb26 for derivation of 82.8% absorption maximum; Derivation of 17.2% reflection minimum and energy conservation analysis; Experimental methodology, supplementary data, and error analysis; Ultrathin absorbers: performance and material selection for diverse spectra; Polarization-selective absorption at grazing incidence; Comparison of mechanisms among strategies for breaking 50% absorption limit.
[42] D. W. Berreman, Optics in stratified and anisotropic media: $4 \times 4$-matrix formulation, J. Opt. Soc. Am. **62**, 502 (1972).
[43] J. B. Pendry, A. J. Holden, D. J. Robbins, and W. J. Stewart, Low frequency plasmons in thin-wire structures, J. Phys.-Condes. Matter **10**, 4785 (1998).
[44] J. Luo, H. Chu, R. Peng, M. Wang, J. Li, and Y. Lai, Ultrabroadband reflectionless Brewster absorber protected by reciprocity, Light-Sci. Appl. **10**, 89 (2021).
[45] H. Fan, H. Chu, H. Luo, Y. Lai, L. Gao, and J. Luo, Brewster metasurfaces for ultrabroadband reflectionless absorption at grazing incidence, Optica **9**, 1138 (2022).
[46] B. Hüttner, On Brewster's angle of metals, J. Appl. Phys. **78**, 4799 (1995).
[47] K. E. Oughstun, Modified Brewster and pseudo-Brewster angles at the interface between isotropic lossy media, J. Opt. Soc. Am. A **37**, 1505 (2020).
[48] M. Neshat and N. P. Armitage, Terahertz time-domain spectroscopic ellipsometry: Instrumentation and calibration, Opt. Express **20**, 29063 (2012).
[49] Z. Mazaheri, C. Koral, and A. Andreone, Accurate THz ellipsometry using calibration in time domain, Sci. Rep. **12**, 7342 (2022).
[50] L. Ding, Q. Y. S. Wu, and J. H. Teng, Polarization independent broadband terahertz antireflection by deep-subwavelength thin metallic mesh, Laser Photonics Rev. **8**, 941 (2014).
[51] A. Thoman, A. Kern, H. Helm, and M. Walther, Nanostructured gold films as broadband terahertz antireflection coatings, Phys. Rev. B **77**, 195405 (2008).
[52] R. Degl Innocenti, H. Lin, and M. Navarro-Cía, Recent progress in terahertz metamaterial modulators, Nanophotonics **11**, 1485 (2022).